## Supporting informations

# Smart responsive luminescence and VOCs sensing application of a copper(I) cluster with novel $P_2CuI_2CuN_2$ core

Ze-Qi Dai,[a] Li Song,**[b] Jun-Er Chen,[a,c] Ding-Feng Jin,[a] Hong-Xiao Jin,[a] Xiao-Lin Guo,[a] Hang-Yan Shen[a] and Wen-Xiang Chai*[a,c]

[a] *College of Materials and Chemistry, China Jiliang University, Hangzhou 310018, P.R. China*

[b] *School of Chemistry and Chemical Engineering, Zhejiang Sci-Tech University, Hangzhou 310018, P.R. China*

[c] *Engineering Research Center of Environment-Friendly Functional Materials, Ministry of Education, Huaqiao University, Xiamen, 361021, P.R. China*

## Tables

Table S1. Crystal Parameters and Structure Refinement Data for **1**.

| | |
|---|---|
| Empirical formula | $C_{63}H_{48}Cu_2I_2N_4O_3P_2$ |
| Formula weight | 1351.87 |
| Temperature/K | 293 |
| Space group | $P2_1/m$ |
| Crystal size(mm) | 0.42×0.32×0.20 |
| Crystal system | monoclinic |
| Unit cell dimensions | |
| a(Å) | 9.9622(12) |
| b(Å) | 23.114(2) |
| c(Å) | 13.108(2) |
| α(°) | 90 |
| β(°) | 111.738(16) |
| γ(°) | 90 |
| V(Å3) | 2803.6(7) |
| Z | 2 |
| $\rho_{calc}$ g/cm$^3$ | 1.601 |
| μ/mm- 1 | 1.967 |
| F(000) | 1344.0 |
| Radiation | MoKα (λ=0.71073) |
| 2θ range for data collection/° | 6.258 to 49.994 |
| Reflections collected | 18427 |
| Independent reflections | 5049 [$R_{int}$ = 0.0916, $R_{sigma}$ = 0.0689] |
| Data/restraints/parameters | 5049/0/357 |
| Goodness-of-fit on F2 | 1.041 |
| Final R indexes [I>=2σ(I)] | $R_1$ =0.0817,w$R_2$ =0.2078 |

| | |
|---|---|
| Final R indexes [all data] | $R_1$ =0.1092,w$R_2$ =0.2274 |
| Largest difference peak/hole/eÅ$^{-3}$ | 1.94/-1.59 |

Table S2. Selected Bond Lengths (Å) and Angles (°) for experimental (crystal) and optimized $S_0$ geometries of **1**.

| Complex **1** | Exp. | Cal. $S_0$ | | Exp. | Cal. $S_0$ |
|---|---|---|---|---|---|
| Cu1–I1 | 2.6126(18) | 2.71409 | Cu1–N1 | 2.110(7) | 2.14024 |
| Cu1–I2 | 2.6175(19) | 2.72022 | Cu1–N1$^{\#1}$ | 2.110(7) | 2.14025 |
| Cu2–I1 | 2.7208(16) | 2.82168 | Cu2–P1 | 2.307(2) | 2.41892 |
| Cu2–I2 | 2.6825(15) | 2.81498 | Cu2–P1$^{\#1}$ | 2.307(2) | 2.41886 |
| | | | | | |
| I1–Cu1–I2 | 110.50(7) | 119.00460 | N1–Cu1–N1$^{\#1}$ | 108.9(4) | 110.08523 |
| I1–Cu1–N1 | 109.53(19) | 107.14070 | I2–Cu1–N1 | 109.2(2) | 106.66972 |
| I1–Cu1–N1$^{\#1}$ | 109.53(19) | 107.13389 | I2–Cu1–N1$^{\#1}$ | 109.2(2) | 106.67345 |
| I1–Cu2–I2 | 105.37(5) | 112.34500 | P1–Cu2–P1$^{\#1}$ | 108.51(15) | 114.26122 |
| I1–Cu2–P1 | 106.70(6) | 107.09988 | I2–Cu2–P1 | 111.82(6) | 108.06603 |
| I1–Cu2–P1$^{\#1}$ | 106.70(6) | 107.10298 | I2–Cu2–P1$^{\#1}$ | 111.82(6) | 108.06510 |
| Cu1–I1–Cu2 | 71.79(5) | 64.31769 | Cu1–I2–Cu2 | 72.33(5) | 64.33271 |
| Cu1–I1–I2–Cu2 | 180.00(6) | 179.99849 | Cu1------Cu2 | 3.128(2) | 2.94792 |

$^{\#1}$Symmetry code: +x, 3/2-y, +z.

Table S3. Selected Bond Lengths (Å) and Angles (°) for optimized $S_0$, $S_1$ and $T_1$ geometries of **1**.

| Complex **1** | Cal. $S_0$ | $S_1$ | $T_1$ | | Cal. $S_0$ | $S_1$ | $T_1$ |
|---|---|---|---|---|---|---|---|
| Cu1–I1 | 2.71409 | 2.68676 | 2.77205 | Cu1–N1 | 2.14024 | 2.08027 | 1.97496 |
| Cu1–I2 | 2.72022 | 2.69487 | 2.77464 | Cu1–N2 | 2.14025 | 2.21576 | 1.97596 |
| Cu2–I1 | 2.82168 | 2.72212 | 2.81161 | Cu2–P1 | 2.41892 | 2.46329 | 2.41590 |
| Cu2–I2 | 2.81498 | 2.70293 | 2.81634 | Cu2–P2 | 2.41886 | 2.41558 | 2.41299 |
| | | | | | | | |
| I1–Cu1–I2 | 119.00460 | 112.03704 | 104.35274 | N1–Cu1–N2 | 110.08523 | 101.56599 | 140.69690 |
| I1–Cu2–I2 | 112.34500 | 110.68774 | 102.24619 | P1–Cu2–P2 | 114.26122 | 115.50801 | 116.04934 |
| Cu1–I1–I2–Cu2 | 179.99849 | 162.48350 | 179.54551 | Cu1------Cu2 | 2.94792 | 3.01094 | 3.46687 |

## Figures

Figure S1 (a) Simulated XRD pattern calculated from single crystal data. (b) Experimental XRD pattern recorded from powder sample of complex **1**.

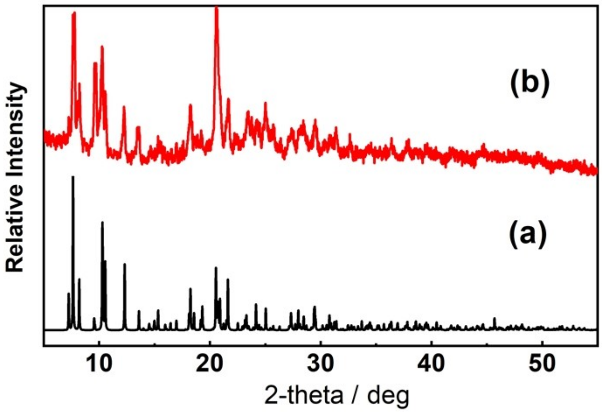

Figure S2 Plot of $F^2(R)$ *vs* photon energy for **1** at room temperature, the estimated bandgap is 2.34 eV.

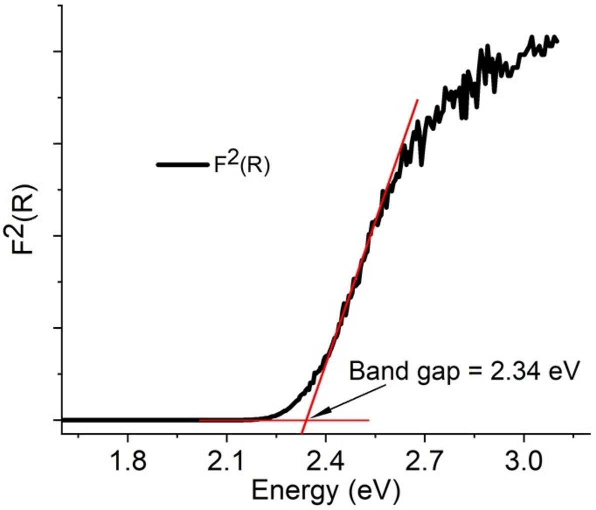

Figure S3 The UV-Vis absorption spectrum for complex **1** in diluted DCM solution at room temperature ($c = 1.0 \times 10^{-5}$ mol / L).

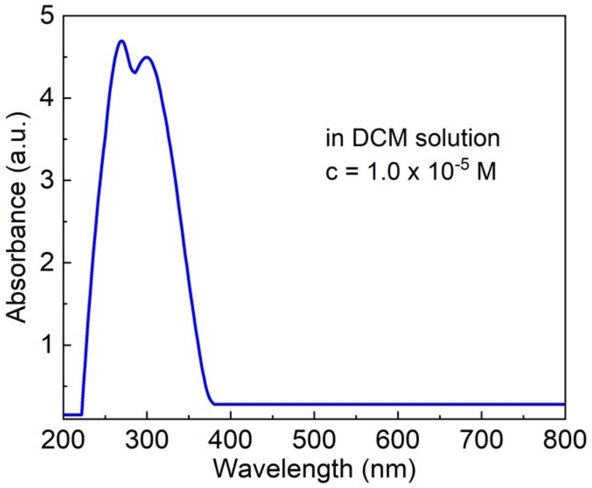

Figure S4 The UV-Vis absorption spectrum for **1** in a PMMA thin film (doped 5%) at room temperature.

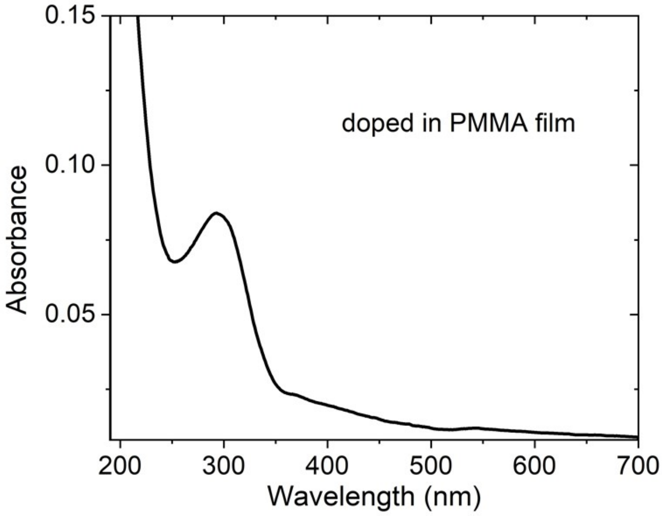

Figure S5 The PL emission spectrum for complex **1** in a PMMA:**1** thin film (doped 5%) at room temperature ($\lambda_{ex}$ = 365 nm).

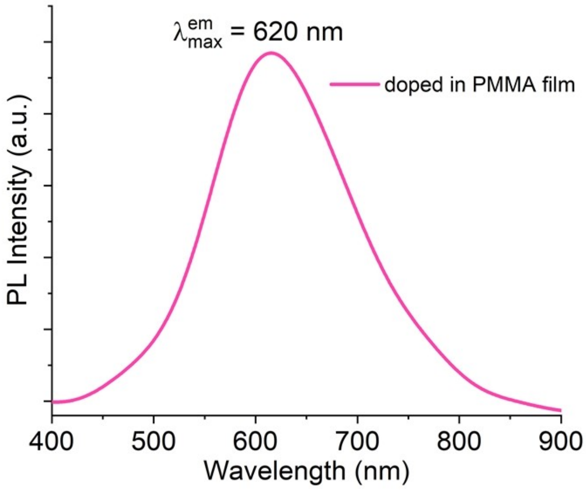

Figure S6 The PL emission spectrum for complex **1** loaded on a test paper ($\lambda_{ex}$ = 365 nm).

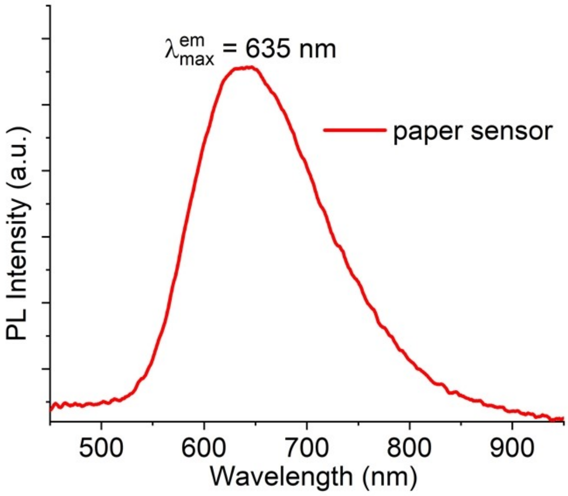

Figure S7 The comparison of experimental geometry from crystal data (green) and optimized geometry from DFT calculation (red), H atoms are omitted for clarity.

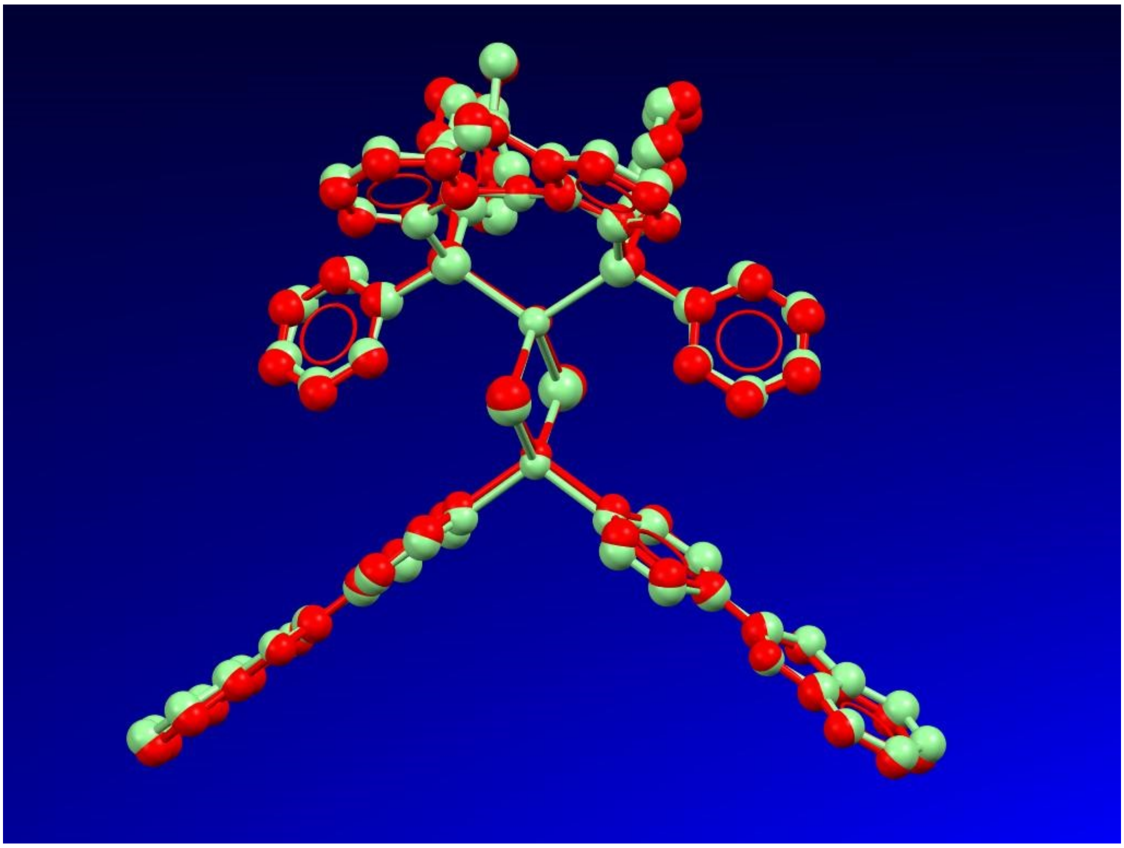

Figure S8 Some Kohn-Sham molecular orbital diagrams involved in the main transition modes of the 10 low-lying excited state in complex **1**. The molecular orbital energies are in atomic units; isovalue = 0.03.

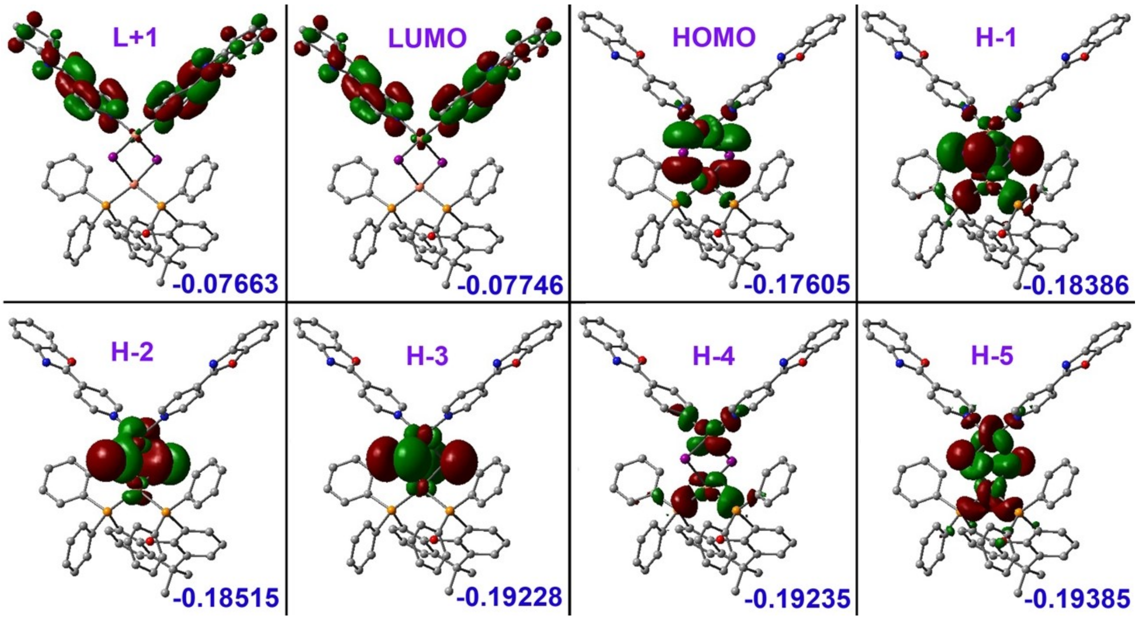

Figure S9 The Kohn-Sham molecular orbital diagrams of the HOMO and LUMO at the $T_1$ minimum for complex **1**. isovalue = 0.03.

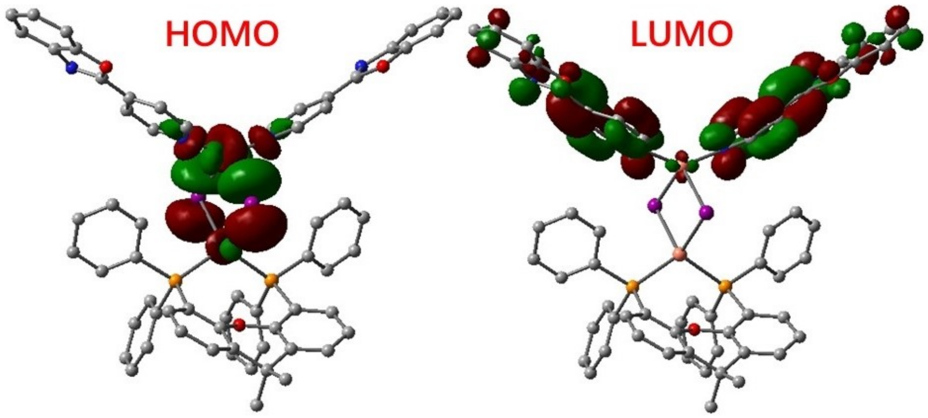

Figure S10 The Kohn-Sham molecular orbital diagrams of the HOMO and LUMO at the $S_1$ minimum for complex **1**. isovalue = 0.03.

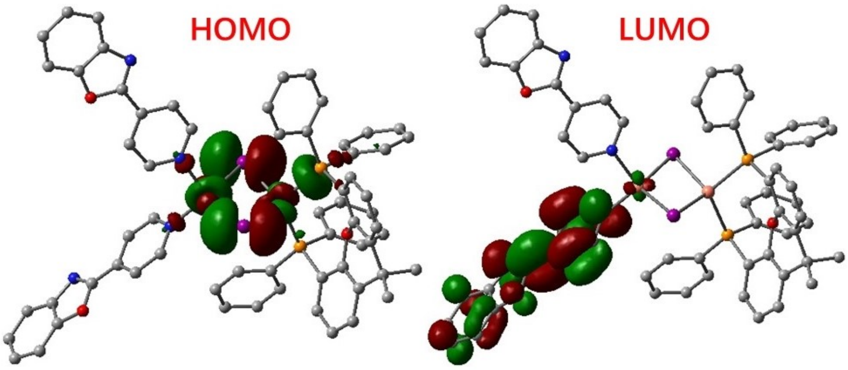

Figure S11 The photographs for the powder of complex **1**under UV irradiation (top) and under natural light (bottom): before (a), and after exposed in pyridine (b) and cyclohexylamine (c) vapours.

Figure S12 The UV-Vis absorption spectra of the three complexes **1**-**3**, obtained through powder diffuse reflection measurement.

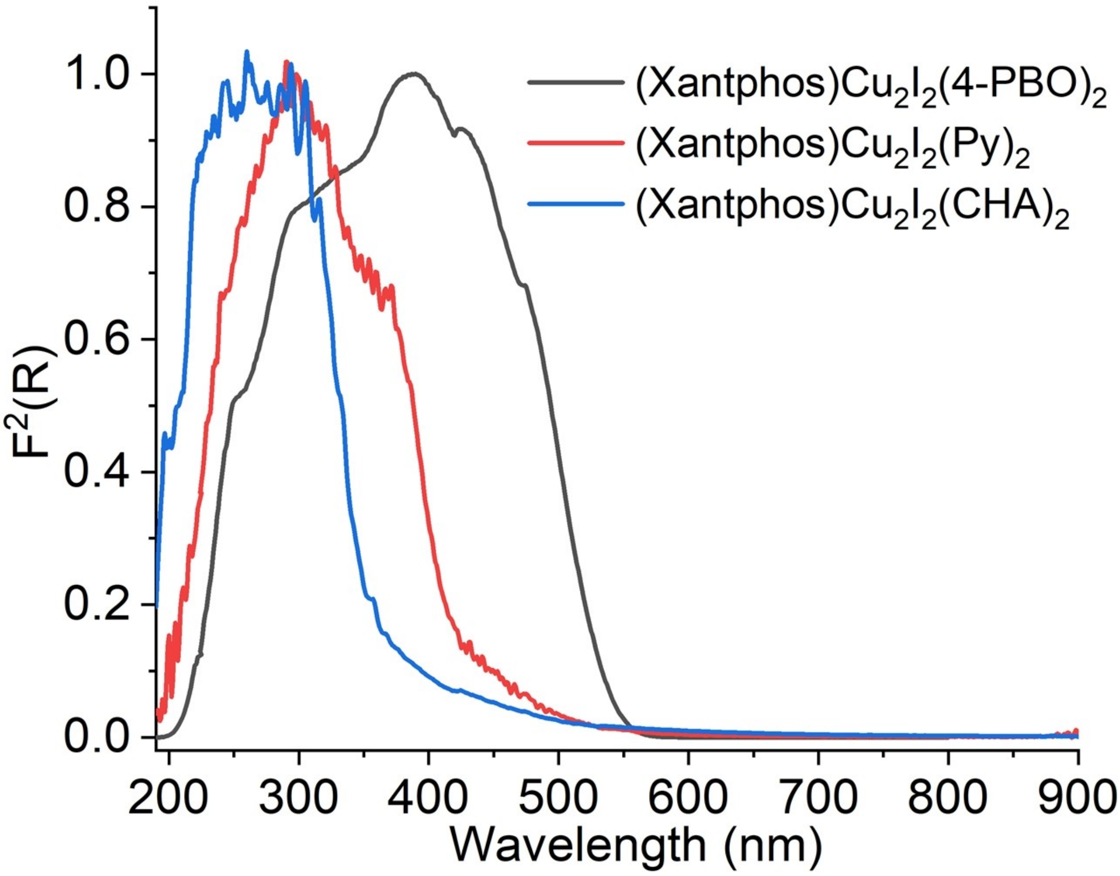

Figure S13 The PL emission spectrum measured on powder sample at room temperature ($\lambda_{ex}$ = 365 nm) for complexes of **2**-**3** and ligand 4-PBO.

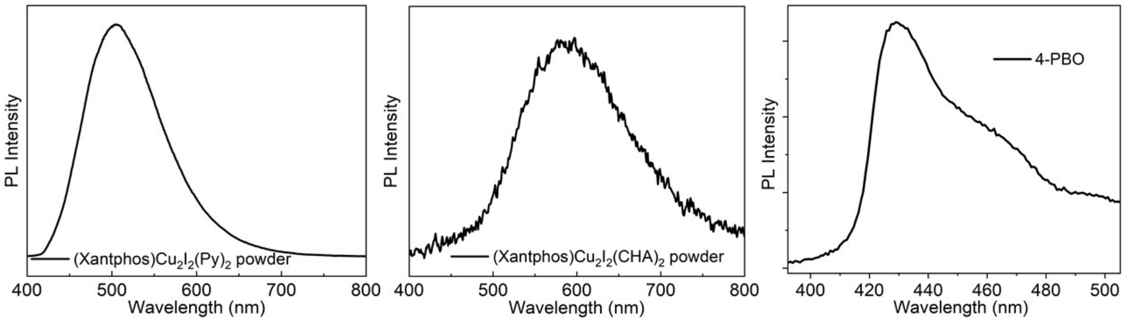

Figure S14 The FTIR spectrum measured on powder samples of complex **1** and its derivatives after exposed in pyridine and cyclohexylamine vapours, and the sample recovered after sensing response.

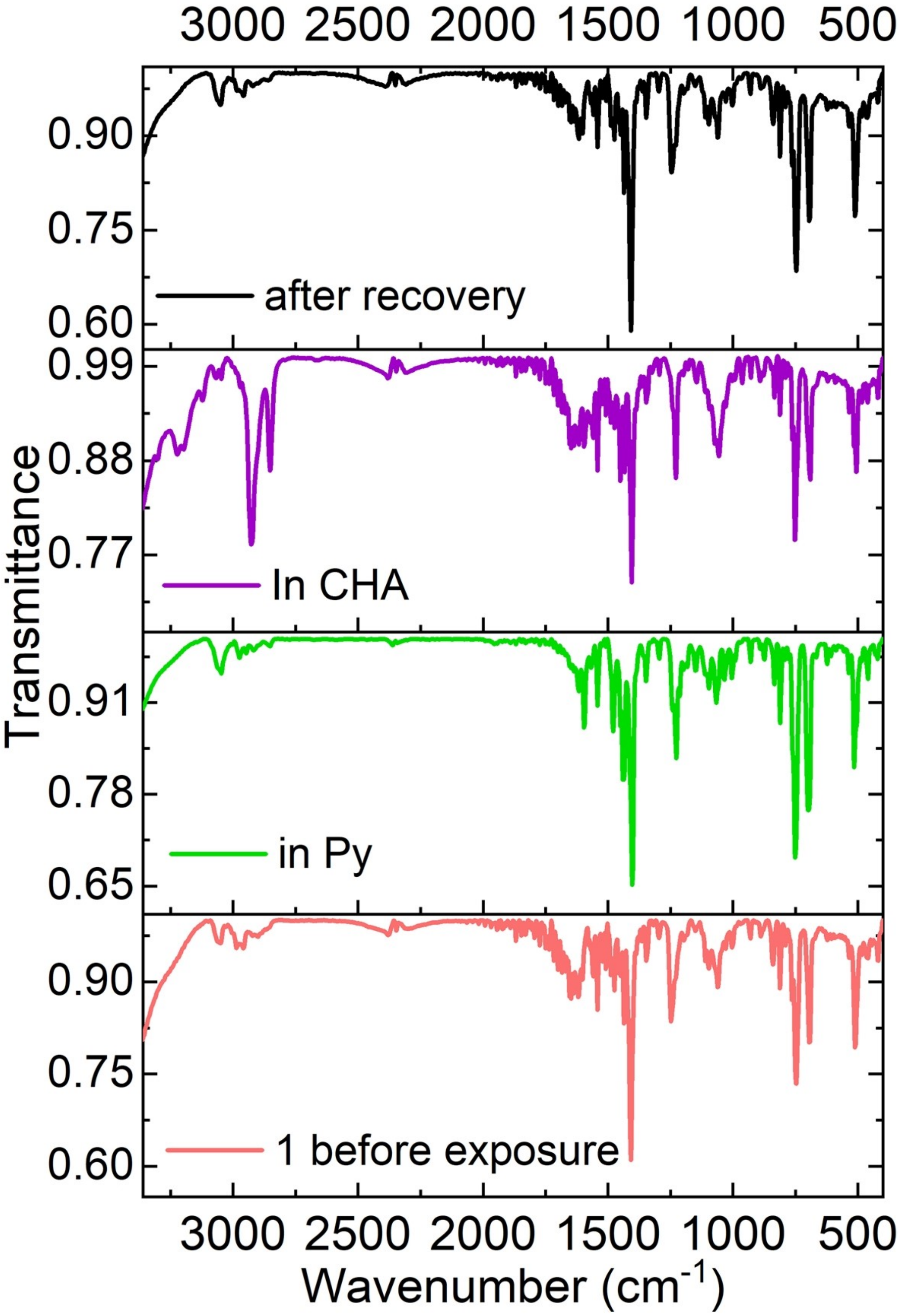

Figure S15 The Kohn-Sham molecular orbital diagrams of the HOMO and LUMO for complex (Xantphos)$Cu_2I_2(Py)_2$ (**2**). isovalue = 0.03.

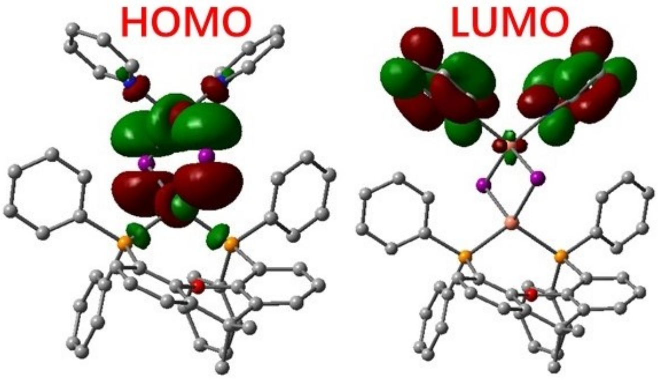

Figure S16 The Kohn-Sham molecular orbital diagrams of the HOMO and LUMO for complex (Xantphos)$Cu_2I_2(CHA)_2$ (**3**). isovalue = 0.03.

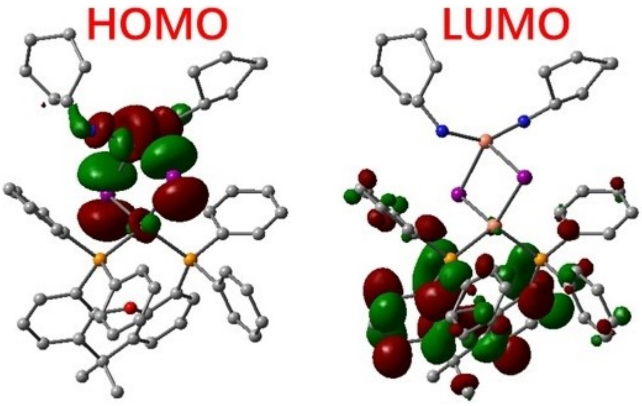

Figure S17 The simulated UV-Vis absorption spectra of **1**-**3**, obtained from TD-DFT calculation.

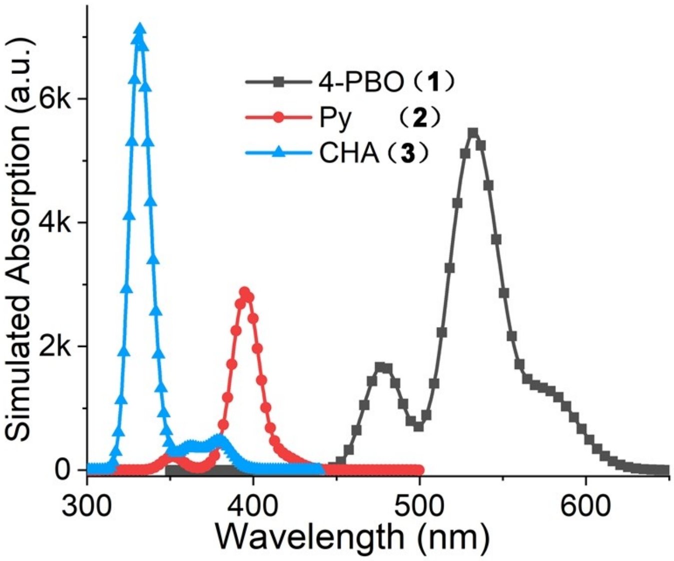

Figure S18 The simulated FTIR spectra of **1**-**3** (from top to bottom), obtained from DFT calculation.

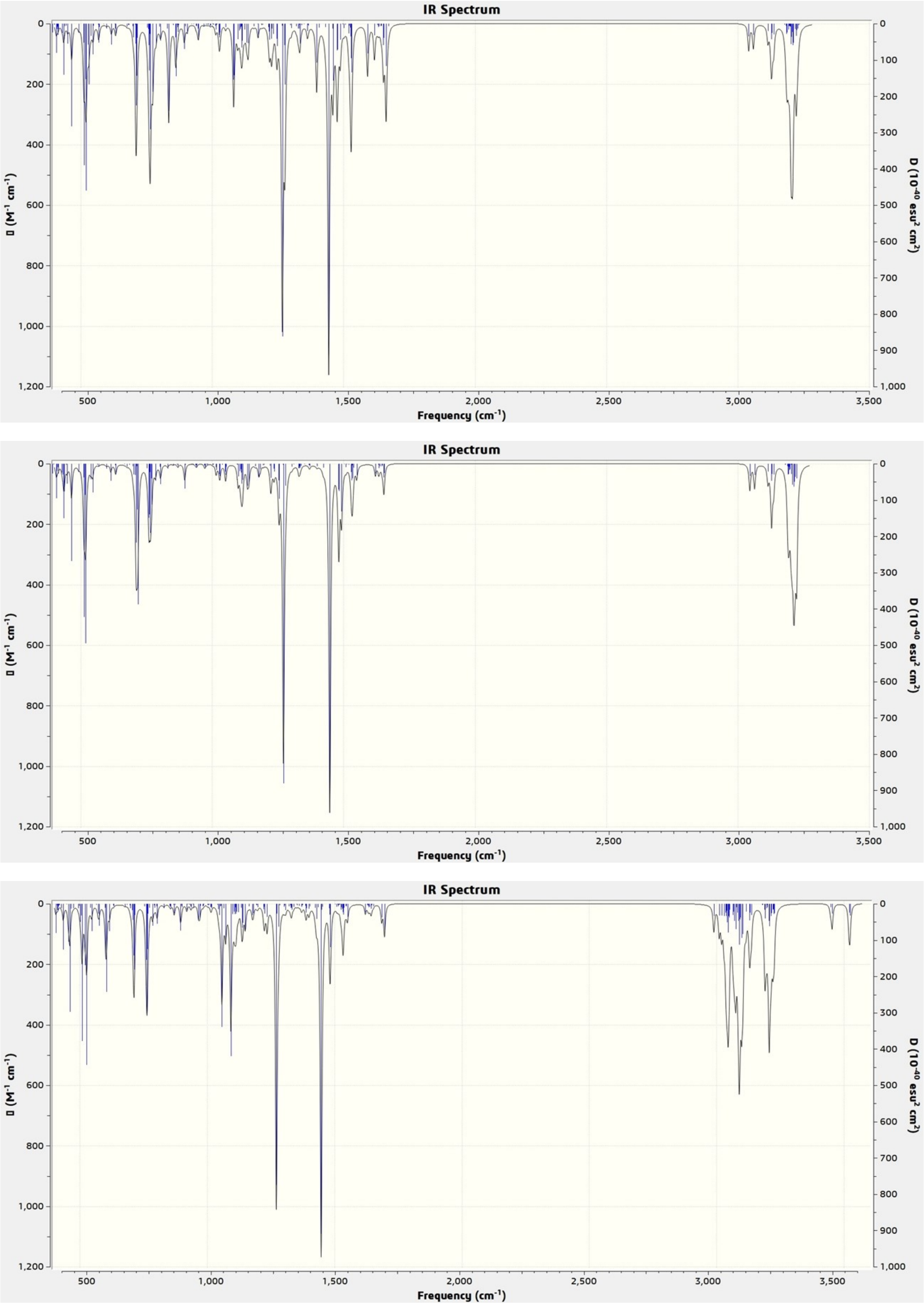

Figure S19 The PL spectral of the paper-based sensor loaded with cluster **1** before and after response in pyridine (Py) vapor, and their recovery by heating.